

Article

Controlling Parameters in the Efficiency of Hydrogen Production via Electrification with Multi-Phase Plasma Processing Technology

Shariful Islam Bhuiyan¹, Kunpeng Wang^{2,*}, Md Abdullah Hil Baky¹, Jamie Kraus¹, Howard Jemison² and David Staack^{1,*}

¹ Department of Mechanical Engineering, Texas A&M University, College Station, TX 77843, USA

² LTEOIL, LLC, 2929 Allen Parkway, Suite 200, Houston, TX 77019, USA

* Correspondence: kpwang@lteoil.com (K.W.); dstaack@tamu.edu (D.S.)

Abstract: A nanosecond pulsed non-equilibrium plasma reactor is used to crack hydrocarbons into hydrogen and lighter intermediates at atmospheric pressure and warm temperature. The effects of power, capacitance, breakdown voltage, pulsing frequency, energy per pulse, and carrier gas type are investigated for product generation. Multiple gaseous products including hydrogen and hydrocarbons are calculated and compared at different conditions. A statistical analysis is performed on hydrogen yield for different experimental conditions to determine the significance of the studied parameters. Comparable hydrogen yields are produced when using methane (4 to 22 g-H₂/kWh) as a carrier gas as compared to argon (7 to 14 g-H₂/kWh). Although, notably, the methane carrier is more selective to hydrogen and sensitive to other operating parameters, the argon is not. Statistical analysis shows that plasma power, capacitance, and energy per pulse appear to influence hydrogen yield while pulsing frequency and breakdown voltage do not. A higher yield of hydrogen is achieved with low plasma power and a low energy per pulse, with a low capacitance for both cases of pure CH₄ and pure Ar. The results show that low plasma power based on a low energy per pulse of <10 mJ is preferable for hydrogen production in a batch reactor. This CO₂-free hydrogen production method produces hydrogen from fossil fuels at less than USD 2/kg in electricity.

Keywords: nanosecond pulsed plasma; cracking of hydrocarbons; hydrogen yield; energy per pulse; fossil fuel



Citation: Bhuiyan, S.I.; Wang, K.; Baky, M.A.H.; Kraus, J.; Jemison, H.; Staack, D. Controlling Parameters in the Efficiency of Hydrogen Production via Electrification with Multi-Phase Plasma Processing Technology. *Energies* **2023**, *16*, 5509. <https://doi.org/10.3390/en16145509>

Academic Editors: Federico Galli, Inès Esma Achouri and Bruna Rego de Vasconcelos

Received: 15 June 2023
Revised: 13 July 2023
Accepted: 19 July 2023
Published: 20 July 2023



Copyright: © 2023 by the authors. Licensee MDPI, Basel, Switzerland. This article is an open access article distributed under the terms and conditions of the Creative Commons Attribution (CC BY) license (<https://creativecommons.org/licenses/by/4.0/>).

1. Introduction

Continuous global population and economic growth, combined with rapid urbanization, have resulted in a massive increase in energy demand [1,2]. The conventional energy supply model is based on depleting hydrocarbon (fossil fuel) energy resources that are geographically dispersed and difficult to extract [3,4]. This process emits enormous Greenhouse Gases (GHGs) in our atmosphere, which is the primary cause of global warming [5–9]. Renewable Energy (RE) resources will be critical in the transition to a more sustainable and clean energy system [10,11]. The elegant idea of storing RE in a storable, transportable, and usable energy carrier such as hydrogen may be the solution [12,13]. In comparison to fossil hydrocarbon fuels, hydrogen is not abundant in nature [14]. It can, however, be produced from many primary energy sources and then used as a fuel in an internal combustion engine or a fuel cell, producing only water as a byproduct and zero carbon emissions [15–17]. As a carbon-free fuel with the highest energy content, hydrogen is widely accepted as an environmentally secondary source of renewable energy in place of fossil fuels. Additionally, when supported by appropriate storage technologies, hydrogen can be used for domestic consumption [18–21]. The primary impediment to using hydrogen gas as a fuel is its scarcity in nature, the requirement for low-cost production methods, and the inherent difficulties in transportation and storage. Many developed

countries' energy development strategies recognize the importance of hydrogen for the future energy economy (e.g., the European Commission's European roadmap for hydrogen and fuel cells [22,23] and the US Department of Energy's "National hydrogen energy roadmap" [24]). Lower production costs and higher production efficiency are two of the DOE's 2020 targets for hydrogen production on a distributed scale. The hydrogen economy and market will also expect exponential growth in the next few decades. For example, one study concludes that the European Union (EU) and the UK could see a hydrogen demand of 2300 TWh (2150–2750 TWh) by 2050. This corresponds to 20–25% of the EU and UK final energy consumption by 2050.

There are numerous processes available for producing H₂, namely conventional and renewable technologies. The first category involves the processing of fossil fuels and includes the hydrocarbon reforming and pyrolysis processes. Steam reforming, partial oxidation, and auto-thermal steam reforming are the chemical techniques used in the hydrocarbon reforming process [25,26]. Currently, the catalytic hydrocarbon reforming process is the most developed and cost-effective method of producing hydrogen. Along with the hydrocarbon, the other reactant in the reforming process is either steam or oxygen, which is referred to as steam reforming or partial oxidation [27,28]. Methane has been the most frequently used hydrocarbon for hydrogen generation to date. However, because the catalytic reforming of methane requires a relatively high temperature (>300 °C), it is limited in some applications, such as vehicles, where a rapid ignition/response is required. Additionally, the deactivation of expensive catalysts caused by coke formation is a problem that must be resolved [29,30]. Green hydrogen made from water electrolysis at low temperatures with renewable electricity is being viewed as the key to decarbonizing the energy sector; its cost, however, is still too high to be widely adopted in industry. The hydrocarbons used in this research including methane and liquid hydrocarbons do not have to be fossil-fuel-based. There is an increasing number of renewable hydrocarbons such as renewable natural gas and biofuel. If we use our technology to produce hydrogen from renewable hydrocarbons, the process will be carbon-negative.

Plasma technologies have progressively gained attention for their use to generate hydrogen due to the following characteristics: easy to turn on and off, better compatibility with a wide range of hydrocarbons, elimination of expensive catalyst and fouling, insensitivity to trace impurities in the gas stream, and compactness [31]. Atmospheric or low-pressure plasmas can be used. While low-pressure plasmas like radio-frequency (RF) or microwave (MW) plasmas have the potential to achieve high hydrocarbon conversion and good H₂ selectivity, the low H₂ production rate and the extra energy required for the vacuum device limit their practical application [32]. Atmospheric plasma can be divided into two forms based on the temperature of the gas: thermal plasma and non-thermal plasma. In a thermal plasma, such as a plasma torch, all charged species (electrons and ions) and neutral species (atoms, molecules, radicals, and excited species) are essentially in thermal equilibrium [33]. The gas temperature ranges from 1000 to 10,000 K. Corona discharge, dielectric barrier discharge (DBD), and surface discharge, on the other hand, exist in a thermally non-equilibrium condition, with the electron temperature (10,000–100,000 K or 1–10 eV) being much greater than the gas temperature (<500 K) [34,35]. Plasma cracking occurs in non-thermal plasma (NTP) reactors when free electrons with a mean energy of 1–10 eV collide with neutral molecules, and break C–C and C–H bonds (with a mean energy of 3–4 eV) [36]. Small, activated radicals are created because of these collisions, which are recombined to produce lighter molecules including hydrogen and small hydrocarbons. Several works have been conducted recently to produce hydrogen using plasma [37–40].

Methane pyrolysis using electricity has gained lots of attention recently because of its low cost and existing infrastructure. Monolith is scaling up a plasma-based methane pyrolysis technology to produce clean hydrogen and high-quality carbon black [41]. Other plasma technologies such as the microwave torch are also being investigated for the same purpose [40,42]. Li et al. used NTP generated in four distinct electric discharges to conduct studies on methane conversion to C₂ hydrocarbons and hydrogen (pulsed streamer

discharges, pulsed spark discharges, pulsed DC DBD, and AC DBD) [43]. Maximum H₂ productions of 51% and 69% of methane conversion were achieved using a needle-to-plate reactor with pulsed spark discharges. Prieto et al. concentrated on batch plasma hydrogen generation. Heavy oil conversion to hydrogen with a selectivity of 70% was investigated using a non-equilibrium plate-to-plate corona discharge reactor [44]. The optimal set of variables led to 70 $\mu\text{L}/\text{J}$ of energy efficiency [45]. Rathore et al. used a micro-ball plasma reactor to process JP-8 liquid and convert it into lighter fuels using a low energy per pulse [46]. Wang et al. developed an electrical method using nanosecond pulsed multiphase plasma to convert fossil fuels at ambient temperature. The researchers used a nanosecond pulsed electrical discharge to partially upgrade n-hexadecane with methane and hydrogen at ambient pressure [47]. This oil conversion process has higher efficiency and significantly lower GHG emissions than traditional technologies. Wang et al. also investigated the role of bubble and impurity dynamics in the electrical breakdown and the relative breakdown voltage and energy deposition in the liquid and gas phase of multiphase hydrocarbon plasmas for in-depth research on hydrocarbon conversion using plasmas [48,49].

This study based on work performed by Wang et al. further investigates the effect of capacitance, breakdown voltage, frequency, energy per pulse, and carrier gas type on hydrogen generation under feasible conditions. Hydrogen yields from using both methane and argon are compared at similar experimental conditions, though insignificant differences are observed. Comparing hydrogen yields by using inert gas (argon) to those by using hydrogen-containing gas (CH₄) helps us understand whether hydrogen is produced from the liquid phase or gas phase, which is beneficial for enhancing hydrogen yields. The hydrogen production yield (g-H₂/kWh) is compared at different experimental conditions. Statistical analysis is performed to determine the significance of the studied parameters. While not necessarily determining the optimum conditions, this paper seeks to identify trends for more efficient generation of hydrogen with low cost and GHG emissions.

2. Materials and Methods

2.1. Experimental Setup

Figure 1 shows the diagram of the experimental setup for hydrogen generation using a nanosecond-pulsed non-equilibrium plasma. A cylindrical glass tube with an outer diameter OD of 1-3/4 inches, wall thickness of 1/8 inches, and length of 1-5/8 inches was sealed on both sides using custom-designed aluminum plates with an o ring in between. The top electrode was a 1/4-inch-diameter stainless-steel round rod that functioned as the ground. The lower electrode was a hollow rod of outer diameter OD 1/8 inches and wall thickness of 0.028 inches, which acted as the high-voltage electrode insulated by dielectric alumina of 0.047 inches in thickness to prevent current from leaking into the oil. The aluminum plate had two circular inserts, one for temperature measurement using a thermocouple thermometer and another for a heating rod controlled with a variable transformer (Model no. SC-10T, 117VAC60Hz). The gap distance was 5 mm between the electrodes and submerged under oil where the discharge occurred. The reactor was oriented vertically with the gas flow from the high-voltage electrode through its hollow column. The exhaust gas outlet was centered at the top of the aluminum plate.

The nanosecond pulsed nonequilibrium plasma was generated by an RC circuit powered by a high-voltage dc power supply (Spellman SL150, 0–50 KV, 3 mA). The resistor was 10 Mohm and the capacitor was a variable parameter as per the design of experiments. The application of DC voltage into the dielectric liquid with gas bubbling results in a self-pulsing circuit when the bubble location and applied voltage are both appropriate. A typical nanosecond discharge is represented by a current pulse with a full width at half the maximum peak current of 20 ns. Generally, within 60 ns, the energy is deposited. Due to the stochastic nature of the bubble discharge initiation process, there is significant variability in both the breakdown voltage and frequency. LabVIEW, a data acquisition system, was used to record the total current and voltage from the power supply and the data were processed using MATLAB 2020b. An oscilloscope (Tektronix model no. DPO 7254C with

a time resolution of 40 GS/s) was also used with a voltage probe and current transducer to study the nanosecond energy deposition events. The energy input into the reactor was determined by using the same method in our previous work [47].

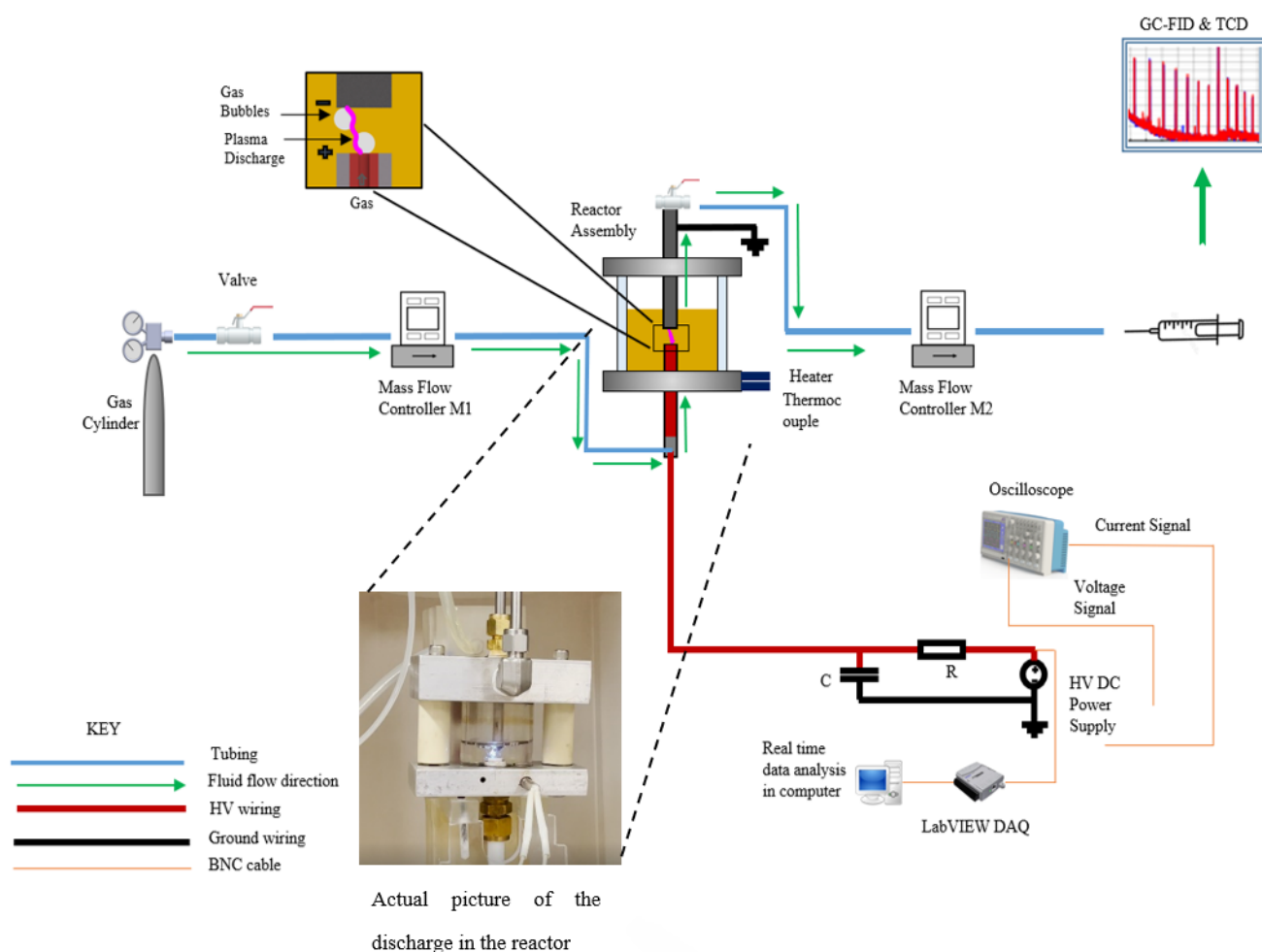


Figure 1. Diagram of the experimental setup for hydrogen generation using a nanosecond-pulsed non-equilibrium plasma with actual picture of the discharge in the reactor.

2.2. Experimental Procedures and Product Analysis

About 9 g (~12 mL) of pure C16 (>99%) from Sigma Aldrich was injected into the reactor, partially filling the glass chamber and filling the discharge gap between the top and bottom electrode. Carrier gas was bubbled into the gap at a rate of 10 SCCM (standard cubic centimeter) through the capillary and controlled using a mass flow controller from Alicat, Tucson, AZ, USA. The temperature of the discharge gap was maintained at 100 °C by heating the bottom plate. A thermocouple was also inserted into the bottom aluminum plate to monitor the temperature. The flow rate of the outlet gas was measured by another mass flow meter and data were logged into its flow controller software. A 50 mL syringe was also used to calculate the volumetric flow rate by recording the time taken to fill the syringe. The syringe was later sampled and analyzed using a Shimadzu gas chromatograph 2014 equipped with a flame ionization detector for detecting hydrocarbons and a thermal conductivity detector for detecting hydrogen. A 27-refinery gas calibration standard was performed to measure the linearity of distinct hydrocarbon gas species and calibrate the instrument to enable molar volume concentration outputs after running a sample.

2.3. Design of Experiments

The experiments were designed to investigate different parameters and their effects on hydrogen production yield on a g-H₂/kWh basis. Three independent parameters including plasma power (roughly 0.1 W, 1 W, and 4 W), capacitance (25 pF, 100 pF, and 440 pF), and carrier gas feed type (methane and argon) were studied while dependent parameters including energy per pulse, frequency, and voltage were also changed. Ideally, 3 × 3 × 2 × 3 = 54 experiments with three repeats need to be conducted to fully investigate the effects of those parameters. However, due to the limit of time and resources, only a fraction of those experiments were conducted to compare hydrogen gas yield at different plasma powers and capacitances with different carrier gases. Four groups of experiments were conducted for pure CH₄, and each group consisted of sets targeting a specific plasma power with capacitance as the independent variable and breakdown voltage and frequency as dependent variables. During the experiments, the target power was approximately controlled by controlling the capacitance, but the voltage and current variation were distinctive. The relation between the parameters was highly nonlinear but still represented the parameter space of target power and capacitance. Similarly, another four groups of experiments were conducted for pure Ar to appropriately compare with the pure CH₄ experiments. Parameters that resulted in optimal hydrogen yield g-H₂/kWh are reported along with the best experimental results. Table 1 below shows the experimental conditions and tested parameters in this paper. Other parameters such as flow rate and residence time, gap length, and bubble dynamics significantly affect the interaction between plasma, gas, and liquid, possibly resulting in different chemistry, but examining these parameters is beyond the scope of this paper.

Table 1. Design of experiments for parametric study.

Carrier Gas	CH ₄					Ar				
Target power (W)	0.1		1		4	0.1		1		4
Capacitance (pF)		25		100	440		25		100	440
	E1		E3	E4	E6	E8		E10	E11	E14
Experiment number	E2			E5	E7	E9			E12	E15
									E13	E16

2.4. Plasma Power Calculation

Plasma power calculation is one of the most important calculations for this work. It is essential to know accurately the power input into the oil. Every time there is an electrical discharge event, the voltage drops and the current spikes. This voltage drop or current spike can be used to count the number of discharge events. A MATLAB code was incorporated into LabVIEW code to count the number of pulses. The MATLAB code uses a function called peakfinder to calculate the pulses. The peakfinder has input arguments to correctly determine the pulse. These arguments include minimum height of the spike and minimum peak prominence (which is the distance the spike falls after an event) amongst others. Data were saved as high fidelity (10,000 samples/s) for power analysis. Counting the number of peaks, which is represented by frequency f , the power delivered into the plasma can be calculated by

$$P = \frac{1}{2} \times C \times V_b^2 \times f$$

$$\text{Energy} = \text{Power} \times \text{time}$$

where C is the capacitance, V_b is the breakdown voltage, and f is the number of pulses per second. The total energy deposited into the system can be calculated by the average power multiplied by the total experimental duration. This is specifically the power added by the plasma to the system.

The hydrogen gas was produced from both the gas phase (in case of CH₄ gas as a carrier gas) and n-C₁₆H₃₄ liquid phase via plasma-induced cracking in all experiments.

The hydrogen yield $\text{g-H}_2/\text{kWh}$ demonstrates the efficiency of producing hydrogen as the ratio of the mass of hydrogen gas produced and the total energy consumed by the reactor and is given by

$$\text{H}_2 \text{ yield} = \frac{\text{Total mass of hydrogen}}{\text{Total energy}}$$

3. Results and Discussion

The pulsed plasma discharges within the liquid and gas phases in the reactor are shown in Figure 1 as an actual image. During a discharge, the nanosecond discharge propagates through the liquid and then along the surface of the bubble and to the counter electrode. This causes chemical conversion of both the gas and liquid phase. After the discharge, a plasma-induced bubble expands and contracts, similar to a cavitation bubble. High-speed videos of the discharges are presented in the supplementary material of Wang et al. [47]. During a discharge, the plasma deposits energy into both the liquid and gas phases, and a proposed model and quantification of energy deposition into each phase have been determined by Wang et al. [49]. A complete mass balance of all the liquid and gas phase products of a single parameter condition was also determined in depth by Wang et al. During the parametric sweeps, the changes in the visual characteristics of the plasma were relatively minor. The discharges were all very short in duration, which caused mixing in the gas–liquid multiphase. Generally, higher pulsing energy and higher plasma power generate brighter light emission and louder sound. This paper focuses on hydrogen production from this multiphase plasma system.

3.1. Product Selectivity

Figure 2 shows the molar selectivity plot for the experiments. Generally, the selectivity toward intermediate hydrocarbons is higher for Ar as a carrier gas compared to methane. Using pure CH_4 as a carrier gas favors more hydrogen selectivity. The highest selectivity for H_2 using CH_4 as a carrier gas is in E2 with 79% selectivity compared to 60% for the Ar case in E9. For experiments with CH_4 as the carrier gas, the multiphase interactions are very complex and distinguishing whether a product arises from the methane or liquid phase cannot be determined. However, it can be concluded that the new gas species concentrations are from both liquid and gas phase interactions with plasma. For Ar as a carrier gas, Ar is an inert gas and, while it can interact as a short-lived radical in the plasma, it does not form stable long-lived compounds with other molecules. Hence, all the gas species products with the Ar carrier are from the liquid phase interaction with plasma. It is possible that some of the product gas hydrocarbon species interact with the liquid phase and generate new molecules. Bubbles are about 2 mm in diameter and, at a flow rate of 10 sccm, have a formation time of ~200 ms. The plasma typically pulses at 10 to 50 Hz (100 ms to 20 ms period between pulses). So, the plasma may interact with a bubble a few times before it exits the discharge zone. Based on this, it is not surprising that the argon discharge is ~10% more selective to produce higher hydrocarbon species than hydrogen. In the methane case, the energy is distributed to both the methane gas and the liquid, producing on average lighter-molecular-weight crack products. The lower C_2H_2 yield in the pure CH_4 case with low capacitance and plasma power compared to higher-capacitance and higher-plasma-power cases in pure CH_4 is also believed to be due to faster energy dissipation and thermal quenching, which suppresses the production of C_2H_2 , which is thermodynamically favored at higher gas temperatures and longer residence times [50,51]. The selectivity in the Ar case remains constant except for E8 where methane production is higher than average. There is more variation in selectivity with the CH_4 case. Although H_2 is the focus of this paper, the other products may also be valuable fuels or chemical/plastic precursor commodities and are efficiently produced by this process. Also, liquid products are generated but not measured for all these cases.

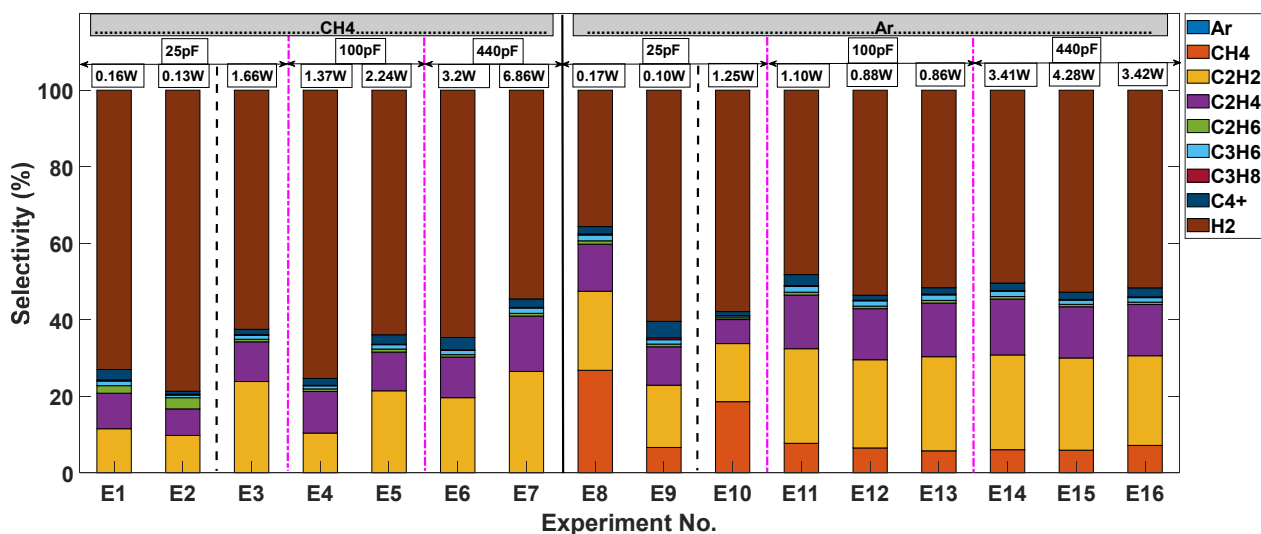


Figure 2. Product selectivity of all experiments with hydrogen and different hydrocarbons. For CH₄ as a carrier gas, methane is not included as a product. For Ar as a carrier gas, methane is also a product. Dash lines are used to differentiate capacitance of tests. Dotted lines are used to differentiate different carrier gas.

3.2. Product Yields

The product mass flow rates ($\mu\text{g/s}$) of various hydrocarbon species and hydrogen gas produced from measured GC-FID/TCD molar concentrations for various plasma powers and capacitances using pure CH₄ with n-C₁₆ (E1–E7) and pure Ar with n-C₁₆ (E8–E16) are also calculated as shown in Figure 3. The mass flow rate is calculated based on both syringe volumetric syringe measurement and mass flow measurement from the mass flow meter and data are validated against each other. Controlled experiments flowing pure CH₄ and Ar in C₁₆ are also performed and plotted as raw values. The raw values act as a baseline for validation of the experiment. The mass flow rate of Ar should remain constant irrespective of the presence of plasma as Ar is an inert gas. For CH₄, it can be produced or consumed in the reaction. It is shown that generally similar hydrocarbon gas species and hydrogen gas are produced compared to the pure Ar cases for similar given plasma powers and capacitances. Achieving high power with low capacitance is quite difficult as a higher frequency is needed to obtain the power and, most times, the spark discharge can transform to a glow. A spark is preferred as it has a significantly higher plasma-to-liquid multiphase interaction than a glow discharge. Hence, the experiment needs to be carefully controlled to ensure the glow mode is not occurring. For a given plasma power, as the power increases, the product mass flow rate of hydrocarbon species increases for both the pure CH₄ and pure Ar cases. The total mass flow of Ar cases is higher than that of CH₄ because Ar weighs more than CH₄. The mass flow rate of pure CH₄ is ~ 100 ($\mu\text{g/s}$) while the mass flow rate of pure Ar is ~ 265 ($\mu\text{g/s}$). The highest mass flow of H₂ is from E7 with the highest power at 12.5 ($\mu\text{g/s}$) with 6.86 W. For Ar as the carrier gas, E13 with 440 pF produces the highest H₂ at 10 ($\mu\text{g/s}$) with 4.28 W. Again, a higher frequency contributes to a higher mass flow of hydrogen with lower capacitance compared to higher capacitance with low frequency. For example, the E3 H₂ production rate is 9.2 ($\mu\text{g/s}$) with 1.66 W compared to E4 at 2.6 ($\mu\text{g/s}$) with 1.37 W. Similarly for Ar, the E10 H₂ production rate is 5.1 ($\mu\text{g/s}$) compared to E11 with 2.6 ($\mu\text{g/s}$).

Figure 4a,b show the relationship between plasma power, total product mass, and H₂ mass. The relationship can be interpreted as a first-order approximation where, as the power increases, both the total mass and H₂ mass increase approximately linearly with an R² value of 0.99 and 0.98 for argon, while E1–E7 with methane as a carrier gas have more variations with an R² value of 0.85. The lower R² value indicates that the process is sensitive to parameters other than power. The Ar set of experiments from E8–E16 tends to

follow the linear trend more closely. For CH₄ as a carrier gas, E1–E7 have some variations and outliers. This is because CH₄ participates in the complex multiphase reaction with plasma and contributes to forming intermediate species, whereas Ar is an inert gas and does not contribute any new products. It also implies that multiphase plasma processing may be more complex when more chemical reactants are present. Nevertheless, in both gases, a higher power deposition contributes to a higher total mass flow and H₂ mass flow. As a function of power, a comparable amount of hydrogen is produced when using methane as a carrier gas as compared to argon. Although, notably, the methane carrier is more sensitive to other operating parameters, the argon is not. The hydrogen yield ranges from 4 to 22 g-H₂/kWh for methane carrier gas and from 7 to 14 g-H₂/kWh for argon carrier gas.

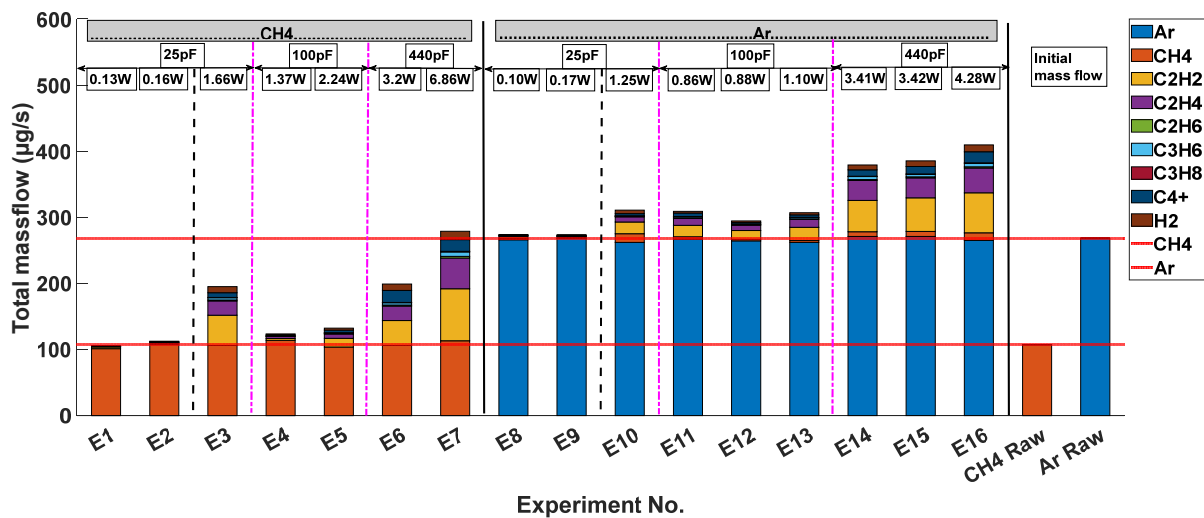


Figure 3. Total mass flow of all experiments with hydrogen and different hydrocarbons. CH₄ raw and Ar raw show initial mass flow. Dash lines are used to differentiate capacitance of tests. Dotted lines are used to differentiate different carrier gas.

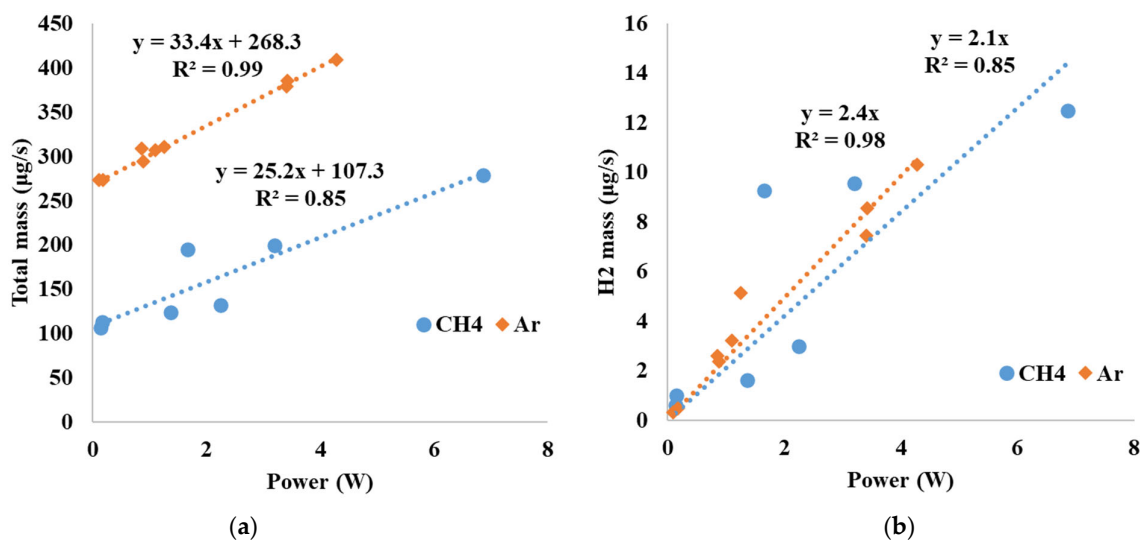


Figure 4. Product mass flow dependence on plasma power. (a) Total mass flow of products changes with plasma power; (b) hydrogen mass flow changes with plasma power. The relationship can be interpreted as a first-order approximation seen as the dotted lines, where as power increases, both the total mass and H₂ mass increase approximately linearly. The goodness of fit is also indicated by the R² value.

3.3. Effect of Different Parameters

3.3.1. Effect of Changing Capacitance

Hydrogen yield ($\text{g-H}_2/\text{kWh}$) is the most important metric to determine the efficiency of the system at producing hydrogen. It is defined as the amount of H_2 produced per kWh of electrical energy consumed. Capacitance is the main independent variable in the experiment. Hydrogen yield and capacitance (pF) for each experiment are plotted in Figure 5 with both CH_4 and Ar as carrier gases. Three power levels (0.1 W, 1 W, and 4 W) are also compared as capacitance changes. Generally, higher hydrogen yields are obtained with a lower capacitance of 25 pF by using CH_4 as the carrier gas. However, a lower capacitance is also susceptible to variations in hydrogen yield. A low capacitance with CH_4 as a carrier gas provides a higher H_2 yield. This could be attributed to the fact that CH_4 also takes part in dissociation reactions and contributes to H_2 yields, while Ar is an inert gas. As capacitance increases, the hydrogen yield decreases rapidly. For Ar, the H_2 yield is consistent for all different capacitance and power levels. For CH_4 , the relation rather has a minimum at 100 pF and then increases at 440 pF. For 100 pF, it is even less than that of Ar. One possible explanation is, as a lower capacitance results in a lower energy per pulse, 25 pF mostly cracks CH_4 molecules into H_2 and not much energy is spent reforming liquids. At a capacitance of 100 pF with a higher pulsing energy, both CH_4 molecules and liquid hexadecane molecules are broken down, resulting in higher H_2 yield. When the capacitance is further increased to 440 pF, pulsing energy may be too high and results in significant gas heating and efficiency loss. The non-equilibrium gas phase mechanism is more efficient at low T_{trans} and high T_{vib} , while equilibrium thermal mechanisms are more efficient at very high T_{trans} . At intermediate conditions, neither equilibrium nor non-equilibrium processes are efficient.

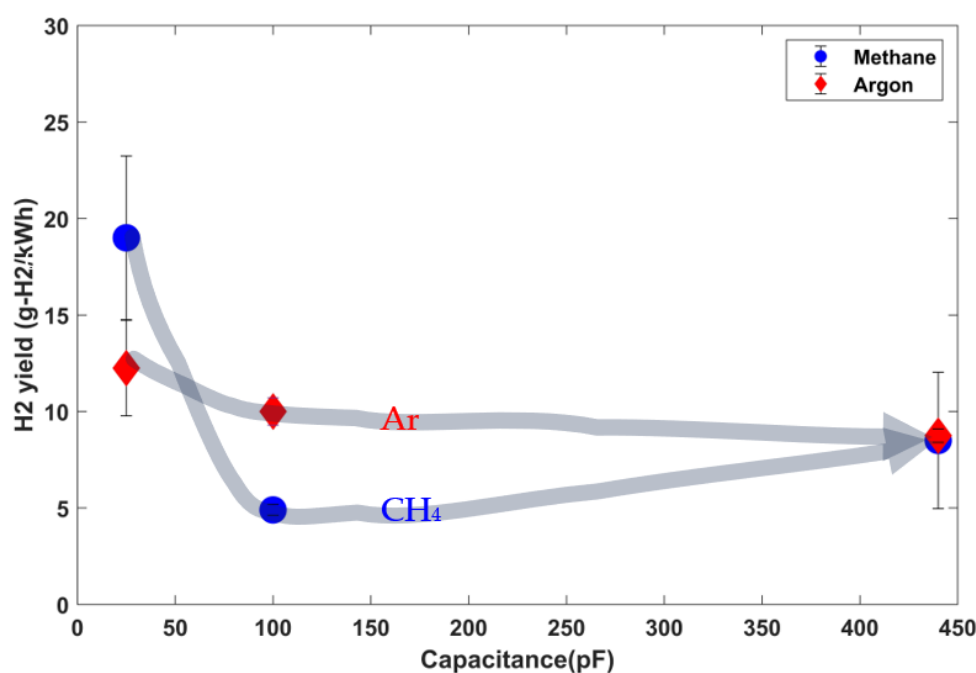


Figure 5. H_2 yield ($\text{g-H}_2/\text{kWh}$) vs. capacitance at different plasma power levels. Capacitance is the main independent variable in the experiment. Plasma power may also change as we change the capacitance, but it is a dependent variable on capacitance.

3.3.2. Effect of Changing Power

Generally, the hydrogen yield decreases as the power is increased and is mainly sensitive at lower powers, as shown in Figure 6a. With power >1 W, the yield flattens out. The best results obtained are the pure CH_4 case, achieving >22 $\text{g-H}_2/\text{kWh}$ at ~ 0.1 W. The

best results for the Ar case are achieving >14 g-H₂/kWh at similar power. The results show that for efficient hydrogen production in a batch system using a pulsed non-thermal plasma, a plasma power less than 0.1 W is preferred. However, the process scale-up for industrial applications will be a challenge due to the extremely low power density of the system. To overcome that, using a continuous-flow system to convert natural gas and liquid fuel would allow much higher plasma powers and still avoid hot gas temperature in the plasma zone because of effective cooling. Systems like such are being developed at the pilot stage.

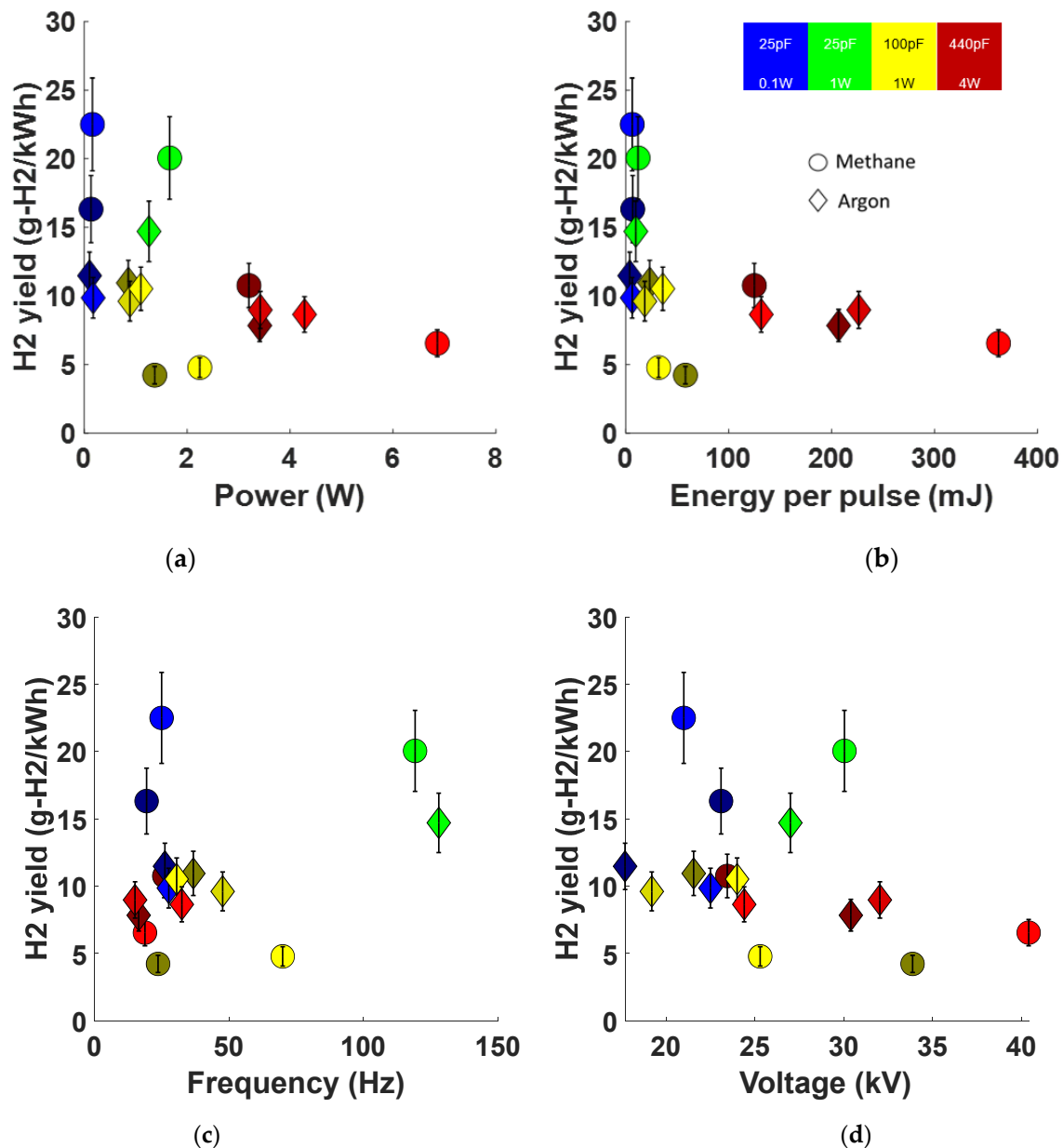


Figure 6. The effect of power, energy per pulse, frequency, and voltage on H₂ yield (g-H₂/kWh). (a) The relation between power and H₂ yield. (b) The relation between energy per pulse and H₂ yield. (c) The relation between frequency and H₂ yield. (d) The relation between voltage and H₂ yield. The horizontal error bars are less than the marker size and hence are not reported here. An increase in power with the same capacitance is represented by a change in color from dark to light.

3.3.3. Effect of Changing Energy per Pulse

Energy per pulse is a derived quantity based upon the capacitance and breakdown voltage given by the following formula:

$$E = \frac{1}{2} \times C \times V^2$$

It represents the energy released during the discharge and may be better correlated with hydrogen yield than primitive variables such as capacitance. A low energy per pulse, e.g., less than 10 mJ, can be deposited by electrical discharge within 100 ns. Molecules may not have enough time to reach thermal equilibrium in such a short time duration, resulting in high vibrational temperature but low gas temperature [52–54]. Generally, the hydrogen yield decreases as the energy per pulse is increased and is mainly sensitive at a lower energy per pulse as shown in Figure 6b. As the energy per pulse increases, more energy is spent in gas heating rather than molecule splitting. A similar trend was observed in work by Delikonstantis [55]. This explains why a lower energy per pulse is more efficient for hydrogen generation. The best results obtained are the pure CH₄ case, achieving >22 g-H₂/kWh at ~6.5 mJ/pulse. The best results for the Ar case are achieving >14 g-H₂/kWh at a similar energy per pulse. The results indicate that for efficient hydrogen production using a pulsed non-thermal plasma, a small energy per pulse less than 10 mJ/pulse is desired.

3.3.4. Effect of Pulsing Frequency and Breakdown Voltage

Generally, the hydrogen yield is not dependent on the pulsing frequency within the range of frequencies tested, as shown in Figure 6c. High yield is obtained in both low-frequency and high-frequency ranges. The best result obtained is the pure CH₄ case with 25 pF (0.1 W plasma power) at <25 Hz and the second-best result is obtained at a much higher frequency of >120 Hz. It is worth mentioning that discharge events are relatively independent from each other at low pulsing frequency. At high frequencies, however, two or more discharge events may deposit energy into the same gas bubble, which causes the gas temperature to increase. At very high frequency, the plasma may transition to a glow-like behavior.

As the voltage is increased, there is a slight decrease in the H₂ yield, as shown in Figure 6d. A higher voltage might be expected to increase the electric field (and reduced electric field E/n), resulting in an improved efficiency of non-equilibrium processes [56,57]. However, that effect might compete with a decrease in non-equilibrium processes due to the increased energy per pulse. Generally, <30 kV of voltage gives a higher H₂ yield. The results >22 g-H₂/kWh show that for efficient hydrogen production using a pulsed non-thermal plasma, a small plasma power ≤0.1 W and a low voltage <30 kV are preferable for high hydrogen yield. At an electrical energy cost of USD 0.038 per kWh, this hydrogen production costs less than USD 2/kg in electricity, which is a milestone for CO₂-free production of hydrogen from fossil fuels.

Table 2 shows the analysis of variance for the different parameters investigated for their effects on hydrogen yields. While some parameter values give higher yield, the statistical significance of the parameters is not very clear from the graphs. Since this is the first time hydrogen yields were studied in a multiphase system using electrical discharges, there are still uncontrolled and unknown parameters in our system. We choose a confidence interval of 90% corresponding to *p* value < 0.1. Our future work will focus on increasing the parameter optimization map to improve data reliability. It shows that capacitance, energy per pulse, and power have a significant response to hydrogen yield, while frequency and voltage do not. The response is inversely correlated with capacitance, power, and energy per pulse, with the statistically significant single-degree-of-freedom coefficients listed in Table 2.

Table 2. Analysis of variance.

Source	DF	Adj SS	Coefficient	F-Value	p-Value
Capacitance	1	81.27	−0.01257	3.76	0.073
Voltage	1	0.000046	NS*	1.9	0.19
Frequency	1	0.000047	NS*	1.95	0.184
Energy per pulse	1	79.93	−0.0218	3.58	0.079
Power	1	81.70	−1.248	3.79	0.072

NS* = Not significant.

3.3.5. Effect of Changing Gas

Comparisons between results from using pure CH₄ and pure Ar as carrier gases for the experimental conditions have shown that the hydrogen gas yield from the liquid phase is significant. In the pure CH₄ experiments, an additional yield of hydrogen gas can be generated from non-oxidative methane gas reforming. The physical and chemical influences of plasma-induced cracking in a multiphase system on the production of hydrogen gas appear to be gas-dependent. The ionization potential and cross-section will vary for different carrier gases; however, a low capacitance will ensure that a low energy per pulse is maintained to maximize energy efficiency for hydrogen gas yield. While a better hydrogen yield can be optimized using both carrier gases with different parameters, the best yields are obtained when using CH₄ as a carrier gas as methane takes part in the multiphase reaction and can act as a hydrogen donor. Ar as a carrier gas has a higher selectivity toward intermediate hydrocarbons than methane. More hydrogen selectivity is favored when pure CH₄ is used as a carrier gas. Pure Ar does not react, so it eventually transfers all its energy to the liquid that is neither in equilibrium nor at a constant temperature. In the methane case, the energy is distributed between the methane gas and the liquid, resulting in crack products that typically have lighter molecular weights. Although H₂ is the focus of this paper, the other products, which are effectively produced by this process, may also be valuable fuel or chemical or plastic precursor commodities.

3.4. Thermodynamics Related to Higher Yield

Best-case results for high hydrogen yield are achieved with low power, low capacitance, and low energy per pulse. Power, energy per pulse, and capacitance, which are statistically significant parameters in these experiments, are strongly correlated. A low power can be achieved using a low energy per pulse, which can be achieved by low capacitance and low voltage. From these results, it is believed that at a low power of ~0.1 W, low capacitance of 25 pF, low voltage of <30 KV, and energy per pulse maintained at <10 mJ/pulse, breakdown events will lead to smaller cavitation bubbles and lower gas temperatures (T_{trans}) but higher vibrational temperatures (T_{vib}) within the bubble vicinity after breakdown compared to higher-energy-per-pulse cases. Smaller bubbles have higher plasma–liquid surface interactions and hence higher probabilities of collisions. A high energy per pulse has a higher power density and higher gas temperature, which will result in more liquid evaporation. Also, a higher energy per pulse has the possibility to overtreat the gas or thermally heat the gas and liquid, wasting energy. All processes are transient and both higher- and lower-energy-per-pulse processes are quenched within microseconds. However, a lower energy per pulse relaxes more rapidly than a higher energy per pulse. In general, at a higher gas translational temperature ($T_{trans} > 2000$ K), thermodynamic equilibrium processes will dominate and have increased efficiency with increasing temperature. On the other hand, at higher vibrational temperature, T_{vib} , non-equilibrium-plasma-driven processes will be more efficient at generating radicals that lead either directly or stepwise to H₂ formation. Hydrogen is a product of both chain scission and cross-linking reactions. Generally, higher vibrational temperature is accessed at high electric field and low gas temperature [58]. With increasing energy per pulse, the rotational and translational temperatures increase, while the vibrational temperature drops. Energy per pulse can also be correlated with pressure in this case. In the lower-pressure region, the

gradient of the rotational temperature is positive, whereas the gradient of the vibrational temperature is negative. Under higher-pressure conditions, both temperatures converge toward a saturation value that is almost equivalent to each other. Vibrational excitation and vibrational relaxation are the two processes that determine the vibrational temperature [58]. As observed from the trends in Figure 5 for methane, the efficiency is higher at low power, low energy per pulse, and low capacitance and then decreases, as seen at 100 pF, and finally increases again at 440 pF. This agrees with the hypothesis that the non-equilibrium gas phase mechanism is more efficient at low T_{trans} and high T_{vib} . Equilibrium thermal mechanisms are more efficient at very high T_{trans} . At intermediate temperatures, neither non-equilibrium nor equilibrium processes are efficient. It should be noted that the mass of hydrogen produced and hydrogen yield are two different parameters during scaling-up to an industrial process, and an optimum might need to exist between either increasing yield or increasing production.

4. Conclusions

A nanosecond pulsed non-equilibrium multiphase plasma reactor is used to convert methane and liquid n-hexadecane into hydrogen and lighter intermediate hydrocarbons at atmospheric pressure and warm temperature. Preliminary results indicate that plasma power, energy per pulse, and carrier gas have larger effects on hydrogen yields than those of breakdown voltage, pulsing frequency, and the other parameters investigated. The product's mass increases mostly linearly with plasma power. As a function of power, a comparable amount of hydrogen is produced when using methane as a carrier gas as compared to argon. Although, notably, the methane carrier is more sensitive to other operating parameters, the argon is not. The selectivity toward hydrogen generation is higher for CH_4 as a carrier gas while the selectivity for intermediate hydrocarbons such as acetylene is higher for Ar as a carrier gas. The hydrogen yield ranges from 4 to 22 g- H_2 /kWh for methane carrier gas and from 7 to 14 g- H_2 /kWh for argon carrier gas. It is shown that a higher yield of g- H_2 /kWh input is achieved with a low energy per pulse, low capacitance, and low breakdown voltage for both cases of pure CH_4 and pure Ar. The results show that for energy-efficient hydrogen production, using a low plasma power of ≤ 0.1 W, low voltage of < 30 kV, and low energy per pulse of < 10 mJ is preferable with CH_4 as a carrier gas and can yield > 22 g- H_2 /kWh. This hydrogen production costs less than USD 2/kg in electricity assuming an electricity cost of USD 0.038 per kWh.

This system is multiphase and is believed to contain a large set of dependent plasma–gas–liquid interaction mechanisms that are influenced by energy per pulse; gas–liquid ratio at the plasma pulse reaction site; liquid and gas temperatures; cavitation bubble temperature; electronic temperatures of neutral, radical, and intermediate species; and collision frequencies. The complexity of this system and the numerous dependencies make determining an overall gas–liquid mechanism challenging. Nevertheless, our results indicated that using this non-equilibrium multiphase plasma system could produce hydrogen at a lower cost than water electrolysis with nearly zero GHG emissions.

Author Contributions: Methodology, K.W.; Validation, K.W., M.A.H.B., J.K. and H.J.; Data curation, S.I.B.; Writing—original draft, S.I.B.; Writing—review & editing, K.W.; Supervision, D.S.; Project administration, D.S.; Funding acquisition, D.S. All authors have read and agreed to the published version of the manuscript.

Funding: This work was sponsored by LTEOIL LLC under Texas A&M Engineering Experiment Station project M1603319.

Data Availability Statement: Data is unavailable due to privacy.

Conflicts of Interest: The authors declare no competing interests.

References

1. World Energy Outlook 2021—Analysis—IEA. Available online: <https://www.iea.org/reports/world-energy-outlook-2021> (accessed on 6 March 2022).
2. National Grid Electricity System Operator. *National Grid Future Energy Scenarios 2019*; Future Energy Scenarios; National Grid Electricity System Operator: London, UK, 2019.
3. Mohtasham, J. Review Article-Renewable Energies. *Energy Procedia* **2015**, *74*, 1289–1297. [[CrossRef](#)]
4. Beiter, P.; Tian, T. *2015 Renewable Energy Data Book*; Barriers to Industrial Energy Efficiency—Report to Congress; National Renewable Energy Lab.(NREL): Golden, CO, USA, 2015; Volume 9.
5. Dincer, I. Renewable Energy and Sustainable Development: A Crucial Review. *Renew. Sustain. Energy Rev.* **2000**, *4*, 157–175. [[CrossRef](#)]
6. Napp, T.A.; Gambhir, A.; Hills, T.P.; Florin, N.; Fennell, P.S. A Review of the Technologies, Economics and Policy Instruments for Decarbonising Energy-Intensive Manufacturing Industries. *Renew. Sustain. Energy Rev.* **2014**, *30*, 616–640. [[CrossRef](#)]
7. Staffell, I.; Scamman, D.; Velazquez Abad, A.; Balcombe, P.; Dodds, P.E.; Ekins, P.; Shah, N.; Ward, K.R. The Role of Hydrogen and Fuel Cells in the Global Energy System. *Energy Environ. Sci.* **2019**, *12*, 463–491. [[CrossRef](#)]
8. Al-Ghussain, L. Global Warming: Review on Driving Forces and Mitigation. *Environ. Prog. Sustain. Energy* **2019**, *38*, 13–21. [[CrossRef](#)]
9. Sévellec, F.; Drijfhout, S.S. Long-Term Global Warming Trend. *Nat. Commun.* **2022**, *9*, 3024. [[CrossRef](#)]
10. Hoppe, T.; de Vries, G. Social Innovation and the Energy Transition. *Sustainability* **2019**, *11*, 141. [[CrossRef](#)]
11. Khezri, M.; Heshmati, A.; Khodaei, M. Environmental Implications of Economic Complexity and Its Role in Determining How Renewable Energies Affect CO₂ Emissions. *Appl. Energy* **2022**, *306*, 117948. [[CrossRef](#)]
12. Rosen, M.A.; Koochi-Fayegh, S. The Prospects for Hydrogen as an Energy Carrier: An Overview of Hydrogen Energy and Hydrogen Energy Systems. *Energy Ecol. Environ.* **2016**, *1*, 10–29. [[CrossRef](#)]
13. Kovač, A.; Paranos, M.; Marciuš, D. Hydrogen in Energy Transition: A Review. *Int. J. Hydrogen Energy* **2021**, *46*, 10016–10035. [[CrossRef](#)]
14. Dawood, F.; Anda, M.; Shafiullah, G.M. Hydrogen Production for Energy: An Overview. *Int. J. Hydrogen Energy* **2020**, *45*, 3847–3869. [[CrossRef](#)]
15. Quarton, C.J.; Samsatli, S. The Value of Hydrogen and Carbon Capture, Storage and Utilisation in Decarbonising Energy: Insights from Integrated Value Chain Optimisation. *Appl. Energy* **2020**, *257*, 113936. [[CrossRef](#)]
16. Shinnar, R. The Hydrogen Economy, Fuel Cells, and Electric Cars. *Technol. Soc.* **2003**, *25*, 455–476. [[CrossRef](#)]
17. Momirlan, M.; Veziroglu, T.N. The Properties of Hydrogen as Fuel Tomorrow in Sustainable Energy System for a Cleaner Planet. *Int. J. Hydrogen Energy* **2005**, *30*, 795–802. [[CrossRef](#)]
18. Elberry, A.M.; Thakur, J.; Santasalo-Aarnio, A.; Larmi, M. Large-Scale Compressed Hydrogen Storage as Part of Renewable Electricity Storage Systems. *Int. J. Hydrogen Energy* **2021**, *46*, 15671–15690. [[CrossRef](#)]
19. Liu, W.; Sun, L.; Li, Z.; Fujii, M.; Geng, Y.; Dong, L.; Fujita, T. Trends and Future Challenges in Hydrogen Production and Storage Research. *Environ. Sci. Pollut. Res.* **2020**, *27*, 31092–31104. [[CrossRef](#)]
20. Kojima, Y. Hydrogen Storage Materials for Hydrogen and Energy Carriers. *Int. J. Hydrogen Energy* **2019**, *44*, 18179–18192. [[CrossRef](#)]
21. Andersson, J.; Grönkvist, S. Large-Scale Storage of Hydrogen. *Int. J. Hydrogen Energy* **2019**, *44*, 11901–11919. [[CrossRef](#)]
22. Van Mierlo, J.; Maggetto, G.; Lataire, P. Which Energy Source for Road Transport in the Future? A Comparison of Battery, Hybrid and Fuel Cell Vehicles. *Energy Convers. Manag.* **2006**, *47*, 2748–2760. [[CrossRef](#)]
23. European Commission HyWays. *The European Hydrogen Roadmap*; Directorate; Directorate-General for Research Information and Communication Unit: Dublin, Ireland, 2008.
24. DOE. *National Hydrogen Energy Roadmap*; DOE: Washington, DC, USA, 2002.
25. Holladay, J.D.; Hu, J.; King, D.L.; Wang, Y. An Overview of Hydrogen Production Technologies. *Catal. Today* **2009**, *139*, 244–260. [[CrossRef](#)]
26. El-Shafie, M.; Kambara, S.; Hayakawa, Y. Hydrogen Production Technologies Overview. *J. Power Energy Eng.* **2019**, *7*, 107–154. [[CrossRef](#)]
27. Xu, J.; Froment, G.F. Methane Steam Reforming, Methanation and Water-gas Shift: I. Intrinsic Kinetics. *AIChE J.* **1989**, *35*, 88–96. [[CrossRef](#)]
28. Rostrup-Nielsen, J.R. Catalytic Steam Reforming. *Catal. Sci. Technol.* **1984**, *5*, 1–117. [[CrossRef](#)]
29. Olabi, A.G.; Bahri, A.S.; Abdelghafar, A.A.; Baroutaji, A.; Sayed, E.T.; Alami, A.H.; Rezk, H.; Abdelkareem, M.A. Large-Vscale Hydrogen Production and Storage Technologies: Current Status and Future Directions. *Int. J. Hydrogen Energy* **2021**, *46*, 23498–23528. [[CrossRef](#)]
30. Nikolaidis, P.; Poullikkas, A. A Comparative Overview of Hydrogen Production Processes. *Renew. Sustain. Energy Rev.* **2017**, *67*, 597–611. [[CrossRef](#)]
31. Chen, H.L.; Lee, H.M.; Chen, S.H.; Chao, Y.; Chang, M.B. Review of Plasma Catalysis on Hydrocarbon Reforming for Hydrogen Production-Interaction, Integration, and Prospects. *Appl. Catal. B* **2008**, *85*, 1–9. [[CrossRef](#)]
32. Czyłkowski, D.; Hrycak, B.; Miotk, R.; Jasiński, M.; Mizeraczyk, J.; Dors, M. Microwave Plasma for Hydrogen Production from Liquids. *Nukleonika* **2016**, *61*, 185–190. [[CrossRef](#)]

33. Jasiński, M.; Czyłkowski, D.; Hrycak, B.; Dors, M.; Mizeraczyk, J. Atmospheric Pressure Microwave Plasma Source for Hydrogen Production. *Int. J. Hydrogen Energy* **2013**, *38*, 11473–11483.
34. Chen, F.F. *Introduction to Plasma Physics and Controlled Fusion*; Plenum Press: New York, NY, USA, 2016.
35. Fridman, A. *Plasma Chemistry*; Cambridge University Press: Cambridge, UK, 2008; Volume 9780521847353.
36. Hooshmand, N.; Rahimpour, M.R.; Jahanmiri, A.; Taghvai, H.; Mohamadzadeh Shirazi, M. Hexadecane Cracking in a Hybrid Catalytic Pulsed Dielectric Barrier Discharge Plasma Reactor. *Ind. Eng. Chem. Res.* **2013**, *52*, 4443–4449. [[CrossRef](#)]
37. Wang, B.; Cheng, Y.; Wang, C.; Zou, J. Steam Reforming of Methane in a Gliding Arc Discharge Reactor to Produce Hydrogen and Its Chemical Kinetics Study. *Chem. Eng. Sci.* **2022**, *253*, 117560. [[CrossRef](#)]
38. Ulejczyk, B.; Nogal, Ł.; Młotek, M.; Krawczyk, K. Enhanced Production of Hydrogen from Methanol Using Spark Discharge Generated in a Small Portable Reactor. *Energy Rep.* **2022**, *8*, 183–191. [[CrossRef](#)]
39. Fan, Z.; Sun, H.; Zhang, S.; Han, W.; Zhang, C.; Yang, Q.; Shao, T. CO_x-Free Co-Cracking of n-Decane and CH₄ to Hydrogen and Acetylene Using Pulsed Spark Plasma. *Chem. Eng. J.* **2022**, *436*, 135190. [[CrossRef](#)]
40. Akande, O.; Lee, B.J. Plasma Steam Methane Reforming (PSMR) Using a Microwave Torch for Commercial-Scale Distributed Hydrogen Production. *Int. J. Hydrogen Energy* **2022**, *47*, 2874–2884. [[CrossRef](#)]
41. Fulcheri, L.; Rohani, V.J.; Wyse, E.; Hardman, N.; Dames, E. An Energy-Efficient Plasma Methane Pyrolysis Process for High Yields of Carbon Black and Hydrogen. *Int. J. Hydrogen Energy* **2023**, *48*, 2920–2928. [[CrossRef](#)]
42. Wang, Q.; Zhu, X.; Sun, B.; Li, Z.; Liu, J. Hydrogen Production from Methane via Liquid Phase Microwave Plasma: A Deoxidation Strategy. *Appl. Energy* **2022**, *328*, 120200. [[CrossRef](#)]
43. Li, X.S.; Zhu, A.M.; Wang, K.J.; Xu, Y.; Song, Z.M. Methane Conversion to C₂ Hydrocarbons and Hydrogen in Atmospheric Non-Thermal Plasmas Generated by Different Electric Discharge Techniques. *Catal. Today* **2004**, *98*, 617–624. [[CrossRef](#)]
44. Wang, K.; Hill, A.; Islam, S.; Kraus, J.; Campbell, C.; Stanich, R.; Jemison, H.; Staack, D. CO₂-Free Conversion of Fossil Fuels by Multiphase Plasma at Ambient Conditions. *Fuel* **2021**, *304*, 121469. [[CrossRef](#)]
45. Kunpeng, W.; David, S.; Howard, J.; Islam, B.S.; Charles, M.; Wang, K.; Staack, D.; Jemison, H.; Bhuiyan, S.I.; Martens, C.; et al. Heavy Oil Cracking Device Scaleup with Multiple Electrical Discharge Modules. U.S. Patent 17/048,635, 19 April 2019.
46. Rathore, K.; Bhuiyan, S.I.S.I.; Slavens, S.M.S.M.; Staack, D. Microplasma Ball Reactor for JP-8 Liquid Hydrocarbon Conversion to Lighter Fuels. *Fuel* **2021**, *285*, 118943. [[CrossRef](#)]
47. Wang, K.; Islam, S.; Hil, A.; Kraus, J.; Campbell, C.; Jemison, H.; Staack, D. Electric Fuel Conversion with Hydrogen Production by Multiphase Plasma at Ambient Pressure. *Chem. Eng. J.* **2021**, *433*, 133660. [[CrossRef](#)]
48. Wang, K.; Bhuiyan, S.I.; Baky, M.A.H.; Kraus, J.; Campbell, C.; Tang, X.; Jemison, H.; Staack, D. Role of Bubble and Impurity Dynamics in Electrical Breakdown of Dielectric Liquids. *Plasma Sources Sci. Technol.* **2021**, *30*, 055013. [[CrossRef](#)]
49. Wang, K.; Bhuiyan, S.I.; Hil Baky, M.A.; Kraus, J.; Campbell, C.; Jemison, H.; Staack, D. Relative Breakdown Voltage and Energy Deposition in the Liquid and Gas Phase of Multiphase Hydrocarbon Plasmas. *J. Appl. Phys.* **2021**, *129*, 123301. [[CrossRef](#)]
50. Kang, H.S.; Lee, D.H.; Kim, K.T.; Jo, S.; Pyun, S.; Song, Y.H.; Yu, S. Methane to Acetylene Conversion by Employing Cost-Effective Low-Temperature Arc. *Fuel Process. Technol.* **2016**, *148*, 209–216. [[CrossRef](#)]
51. Dinh, D.K.; Lee, D.H.; Song, Y.H.; Jo, S.; Kim, K.T.; Iqbal, M.; Kang, H. Efficient Methane-to-Acetylene Conversion Using Low-Current Arcs. *RSC Adv.* **2019**, *9*, 32403–32413. [[CrossRef](#)] [[PubMed](#)]
52. Van Surksum, T.L. Fundamental Investigations of Hydrocarbon Plasma Chemistry. Ph.D. Thesis, Colorado State University, Fort Collins, CO, USA, 2020.
53. Maqueo, P.D.G.; Coulombe, S.; Berghthorson, J.M. Energy Efficiency of a Nanosecond Repetitively Pulsed Discharge for Methane Reforming. *J. Phys. D Appl. Phys.* **2019**, *52*, 274002. [[CrossRef](#)]
54. Sun, H.; Zhang, S.; Gao, Y.; Huang, B.; Zhang, C.; Shao, T. Non-Oxidative Methane Conversion in Diffuse, Filamentary, and Spark Regimes of Nanosecond Repetitively Pulsed Discharge with Negative Polarity. *Plasma Process. Polym.* **2019**, *16*, 1900050. [[CrossRef](#)]
55. Delikonstantis, E.; Scapinello, M.; Van Geenhoven, O.; Stefanidis, G.D. Nanosecond Pulsed Discharge-Driven Non-Oxidative Methane Coupling in a Plate-to-Plate Electrode Configuration Plasma Reactor. *Chem. Eng. J.* **2020**, *380*, 122477. [[CrossRef](#)]
56. Gutsol, A.; Rabinovich, A.; Fridman, A. Combustion-Assisted Plasma in Fuel Conversion. *J. Phys. D Appl. Phys.* **2011**, *44*, 274001. [[CrossRef](#)]
57. Lee, D.H.; Kim, K.T.; Song, Y.H.; Kang, W.S.; Jo, S. Mapping Plasma Chemistry in Hydrocarbon Fuel Processing Processes. *Plasma Chem. Plasma Process.* **2013**, *33*, 249–269. [[CrossRef](#)]
58. Rathore, K.; Wakim, D.; Chitre, A.; Staack, D. Glow Discharge Characteristics of Non-Thermal Microplasmas at above Atmospheric Pressure. *Plasma Sources Sci. Technol.* **2020**, *29*, 055011. [[CrossRef](#)]

Disclaimer/Publisher’s Note: The statements, opinions and data contained in all publications are solely those of the individual author(s) and contributor(s) and not of MDPI and/or the editor(s). MDPI and/or the editor(s) disclaim responsibility for any injury to people or property resulting from any ideas, methods, instructions or products referred to in the content.